

Path Integrals for Nonadiabatic Dynamics: Multistate Ring Polymer Molecular Dynamics

Ananth, Nandini ¹

¹Department of Chemistry and Chemical Biology, Cornell University, Ithaca, NY, USA, 14853; email: ananth@cornell.edu

Xxxx. Xxx. Xxx. Xxx. YYYY. AA:1–26

[https://doi.org/10.1146/\(\(please add article doi\)\)](https://doi.org/10.1146/((please add article doi)))

Copyright © YYYY by Annual Reviews.
All rights reserved

Keywords

nonadiabatic dynamics, path integrals, semiclassical theory, mapping variables, real-time correlation functions, excited state dynamics

Abstract

This review focuses on a recent class of path integral based methods that simulate nonadiabatic dynamics in the condensed phase using only classical molecular dynamics trajectories in an extended phase space. Specifically, a semiclassical mapping protocol is used to derive an exact, continuous, Cartesian variable, path-integral representation for the canonical partition function of a system where multiple electronic states are coupled to nuclear degrees of freedom. Building on this exact statistical foundation, Multistate Ring Polymer Molecular Dynamics methods are developed for the approximate calculation of real-time thermal correlation functions. The remarkable promise of these multistate ring polymer methods, their successful applications, and their limitations are discussed in detail.

Contents

1. INTRODUCTION	2
2. Theory	3
2.1. Nonadiabatic Dynamics	3
2.2. Mapping variables for electronic states	4
2.3. Imaginary-time path integrals for a multistate system	5
2.4. Approximate real-time correlation functions	8
2.5. Exact Quantum Liouvillian in the Mapping Variable Representation	12
3. Implementation	14
3.1. Thermal Correlation Functions	14
3.2. Estimators	14
3.3. Nonequilibrium Correlation Functions	15
4. Applications	16
4.1. Two-level systems	16
4.2. Excited State Dynamics	16
4.3. Mechanistic study of Proton-Coupled Electron Transfer	18
5. Limitations	19
5.1. Reaction Rate Theory	19
5.2. Detailed Balance and Rabi Oscillations	20
5.3. Ab-initio Path Integrals for Nonadiabatic Dynamics	20
5.4. Borrowing limitations from RPMD	20
6. Outlook	20

1. INTRODUCTION

Coupled electron-nuclear motion, nonadiabatic effects, are ubiquitous in chemistry playing a key role in the transport of spin, charge, energy, and excitation through complex molecular systems (1, 2). Adiabatic or Born-Oppenheimer dynamics describe time-evolution of the nuclear wavefunction under forces from a single electronic potential energy surface (3). Nonadiabatic processes, where the Born-Oppenheimer approximation is no longer valid, correspond to nuclear dynamics on multiple, coupled, electronic potential energy surfaces that are no longer energetically well separated. It is this need to include more than one electronic state that offers a challenge to theory: accurate and rapid electronic structure methods are required to characterize multiple electronic states (typically the ground state and a handful of low-lying excited states) accompanied by quantum dynamic methods that can capture the coupling between nuclear motion and electronic state transitions.

Great strides have been made in the development of exact quantum dynamic methods (4, 5, 6, 7, 8), however large scale and predictive simulations of nonadiabatic processes remains a significant challenge. Nonadiabatic methods based on Gaussian wavepacket dynamics (9, 10), and Semiclassical theory have had some success in small system simulations (11, 12, 13, 14), with the Linearized Semiclassical Initial Value Representation (LSC-IVR) (15, 16, 17, 18, 19, 20, 21) and the recently introduced quasi-classical windowing methods (22, 23, 24) showing the most promise for higher dimensional system studies. Similarly, rigorous mixed quantum classical approximations for nonadiabatic dynamics derived from first principles enable studies on systems with a handful of degrees of freedom (25, 26, 27, 28), but it is the more *ad hoc* surface hopping approach that is, arguably, the most widely used for large scale

simulations (29, 30, 31, 32, 33, 34). Unfortunately, standard surface hopping simulations of high-dimensional condensed phase systems face challenges due to the lack of nuclear quantization, the differential treatment of electronic and nuclear dynamics, and the use of dynamics that do not preserve detailed balance (31).

Centroid Molecular Dynamics (CMD) (35, 36, 37, 38) and Ring Polymer Molecular Dynamics (RPMD) (39, 40, 41) have emerged as a particularly successful class of methods for condensed phase simulations of Born-Oppenheimer dynamics. Both these approaches are based on an exact, imaginary-time path integrals (42, 43), and have been shown to successfully describe nuclear quantum effects in condensed phase quantum systems using only classical molecular dynamics trajectories. In particular, RPMD has been used in large scale atomistic simulations of charge transfer (44, 45, 46, 47, 48, 49). The broad success of RPMD has motivated the development of several approximate, imaginary-time path integral based methods for quantum dynamic simulations of nonadiabatic reactions. This includes the Mapping-Variable (MV)-RPMD method that, like RPMD, employs an ensemble of classical trajectories to preserve the quantum Boltzmann distribution (50, 51, 52, 53, 54), and the closely related Nonadiabatic NRPM (55, 56, 57, 58) and Coherent-State (CS)-RPMD (59).

This review showcases the development of multistate RPMD methods, highlighting their promise for efficient, accurate, and predictive simulations of nonadiabatic processes. Current theoretical limitations and implementation challenges are also discussed along with some directions for future development. Readers of this review might find it helpful to refresh their understanding of nonadiabatic dynamics and conical intersections (60) as well as RPMD (41).

2. Theory

2.1. Nonadiabatic Dynamics

The molecular Hamiltonian for a system of electrons and nuclei can be written as

$$\hat{H}(\mathbf{r}, \mathbf{R}) = \hat{T}_R + \hat{H}_{\text{el}}(\mathbf{r}, \mathbf{R}), \quad 1.$$

where \hat{T}_R is the nuclear kinetic energy operator and $\hat{H}_{\text{el}}(\mathbf{r}, \mathbf{R})$ is the electronic Hamiltonian operator. The eigenfunctions of the total molecular Hamiltonian can then be written as an expansion,

$$\Psi(\mathbf{r}, \mathbf{R}, t) = \sum_j \chi_j(\mathbf{R}, t) \phi_j(\mathbf{r}, \mathbf{R}), \quad 2.$$

where the time-dependent nuclear wavefunction are the coefficients of expansion, $\chi_j(\mathbf{R}; t)$, and $\phi_j(\mathbf{r}, \mathbf{R})$ are the complete orthonormal set of eigenfunctions obtained by solving the time-independent electronic Schrödinger equation,

$$\hat{H}_{\text{el}} \phi_j(\mathbf{r}, \mathbf{R}) = E_j(\mathbf{R}) \phi_j(\mathbf{r}, \mathbf{R}), \quad 3.$$

The total molecular wavefunction evolves in time according to the time-dependent Schrödinger equation,

$$i\hbar \frac{d\Psi(\mathbf{r}, \mathbf{R}, t)}{dt} = H(\hat{\mathbf{r}}, \hat{\mathbf{R}}) \Psi(\mathbf{r}, \mathbf{R}, t), \quad 4.$$

that can be further simplified to obtain equations of motion for the nuclear wavefunction,

$$i\hbar \frac{d\chi_j(\mathbf{R}, t)}{dt} = \left[\hat{T}_R + E_j(\mathbf{R}) \right] \chi_j(\mathbf{R}, t) + \sum_k C_{jk}. \quad 5.$$

Equation 5 describes coupled *nonadiabatic* motion of the nuclear wavefunction $\chi_j(\mathbf{R}, t)$: the first term in square parentheses defines motion on a single electronic potential energy surface $E_j(\mathbf{R})$ and the second term describes coupled motion through the nonadiabatic coupling operator,

$$C_{jk} = \langle \phi_j | \hat{T}_R | \phi_k \rangle - \sum_i \frac{\hbar^2}{M_i} \langle \phi_j | \nabla_i | \phi_k \rangle \nabla_i, \quad 6.$$

where nuclear kinetic operator is $\hat{T}_R = -\sum_i \frac{\hbar^2}{2M_i} \nabla_i^2$, and the summation index i runs over the number of nuclear degrees of freedom. Born-Oppenheimer dynamics (sometimes referred to as adiabatic dynamics) assumes that the nonadiabatic coupling is negligible, i. e. $C_{jk} \approx 0$, resulting in a significantly simpler equation that describes nuclear motion on a single electronic surface (3).

Adiabatic and Diabatic Representations

In general, the complete set of eigenfunctions of the electronic Hamiltonian, $\{\phi_j(\mathbf{r}, \mathbf{R})\}$ are referred to as the *adiabatic* representation, and as discussed above, nuclear motion is coupled to the adiabatic electronic states through the nonadiabatic coupling vector. This vector is challenging to compute for high-dimensional systems and its magnitude is inversely proportional to the energetic separation between electronic states making it singular at conical intersections.

The *diabatic* representation is constructed to minimize the nonadiabatic coupling vector. However, the resulting states are not eigenstates of the electronic Hamiltonian leading to off-diagonal terms in the potential energy matrix. Diabatic states are frequently localized, providing an intuitive physical picture of reactive events: for instance, the ‘donor state’ and the ‘acceptor state’ in an electron transfer reaction are, typically, diabats.

Diabatic states are non-unique and several diabaticization protocols have been developed to construct quasi-diabatic states either by transforming from an adiabatic basis or through direct localization protocols (61, 62, 63, 64, 65, 66, 67, 68, 69). The multistate RPMD methods discussed here are all derived assuming a diabatic representation.

2.2. Mapping variables for electronic states

Developing classical trajectory based methods for nonadiabatic dynamics requires transforming from discrete electronic states to continuous Cartesian electronic variables. This idea has been explored extensively in the semiclassical literature and several formally exact mappings have been proposed (11, 12, 70, 71). This review confines itself to the Meyer-Miller-Stock-Thoss (MMST) mapping that has been shown to work well for a wide range of applications (19, 13, 18, 72, 73).

The MMST mapping was first introduced as a mapping from discrete electronic state variables to classical analog action-angle variables (11, 74), and subsequently established to be an exact transformation (12). Specifically, electronic states are mapped to bosonic creation and annihilation operators with commutation relations $[a_n^\dagger, a_m] = \delta_{nm}$,

$$|\psi_n\rangle \langle \psi_m| \rightarrow \hat{a}_n^\dagger \hat{a}_m = \frac{1}{\sqrt{2\hbar}} ([\hat{\mathbf{x}}]_n - i[\hat{\mathbf{p}}]_n) \frac{1}{\sqrt{2\hbar}} ([\hat{\mathbf{x}}]_m + i[\hat{\mathbf{p}}]_m). \quad 7.$$

In Equation 7, $[\cdot]_n$ indicates the n^{th} element of the K -dimensional electronic position and momentum operators, $\hat{\mathbf{x}}$ and $\hat{\mathbf{p}}$, and the equality is obtained using the definitions of the

ladder operators. The K electronic states of the system are thus mapped to a set of K singly excited oscillator (SEO) states,

$$|\psi_n\rangle \rightarrow |0_1 0_2 \dots 1_n \dots 0_K\rangle \equiv |n\rangle, \quad 8.$$

that are defined as the product of $K - 1$ independent ground state harmonic oscillators and one oscillator in the first excited state. In Equation 8, the notation $|n\rangle$ is introduced for the SEO states indicating that the n^{th} oscillator is singly excited. As a simple example, the electronic states of a two-level system can be mapped to two SEO states, $|1\rangle$ and $|2\rangle$, such that

$$\psi_1 \rightarrow |1\rangle \equiv |1_1 0_2\rangle \text{ and } \psi_2 \rightarrow |2\rangle \equiv |0_1 1_2\rangle. \quad 9.$$

Note that the mapping defined here is exact for both adiabatic and diabatic states. (11, 18).

Now, consider a diabatic Hamiltonian for a system with K electronic states and F nuclear degrees of freedom,

$$\hat{H} = \frac{1}{2} \hat{\mathbf{P}}^T \mathbf{M}^{-1} \hat{\mathbf{P}} + V_0(\hat{\mathbf{R}}) + \sum_{n,m=1}^K |\psi_n\rangle [\mathbf{V}_e]_{nm}(\hat{\mathbf{R}}) \langle \psi_m|, \quad 10.$$

where \mathbf{R} and \mathbf{P} are the F -dimensional vectors of nuclear positions and momenta, \mathbf{M} is the diagonal mass matrix, $V_0(\mathbf{R})$ is the state-independent potential energy, $[\mathbf{V}_e]_{nm}(\mathbf{R})$ are elements of the $K \times K$ diabatic potential energy matrix, and $|\psi_n\rangle$ are the diabatic electronic states. Using the mapping in Equation 7, it is possible to write the K -state Hamiltonian in Equation. 10 in the SEO basis as

$$\hat{H} = \frac{1}{2} \hat{\mathbf{P}}^T \mathbf{M}^{-1} \hat{\mathbf{P}} + V_0(\hat{\mathbf{R}}) + \sum_{n,m=1}^K |n\rangle [\mathbf{V}_e]_{nm}(\hat{\mathbf{R}}) \langle m|, \quad 11.$$

or equivalently in Cartesian operator form

$$\hat{H}_{\text{mmst}} = \frac{1}{2} \hat{\mathbf{P}}^T \mathbf{M}^{-1} \hat{\mathbf{P}} + V_0(\hat{\mathbf{R}}) + \frac{1}{2} \sum_{n,m=1}^K [\mathbf{V}_e]_{nm}(\hat{\mathbf{R}}) ([\hat{\mathbf{x}}]_n [\hat{\mathbf{x}}]_m + [\hat{\mathbf{p}}]_n [\hat{\mathbf{p}}]_m - \delta_{nm} \hbar) \quad 12.$$

Approximate semiclassical methods for nonadiabatic dynamics like LSC-IVR (15, 16, 17, 19) typically use classical trajectories generated by the Hamiltonian in Equation 12,

$$\begin{aligned} \dot{\mathbf{R}} &= \frac{\partial H_{\text{mmst}}}{\partial \mathbf{P}} & \dot{\mathbf{P}} &= -\frac{\partial H_{\text{mmst}}}{\partial \mathbf{R}} \\ [\dot{\mathbf{x}}]_n &= \frac{\partial H_{\text{mmst}}}{\partial [\mathbf{p}]_n} & [\dot{\mathbf{p}}]_n &= -\frac{\partial H_{\text{mmst}}}{\partial [\mathbf{x}]_n} \end{aligned} \quad 13.$$

2.3. Imaginary-time path integrals for a multistate system

The path integral representation yields an exact classically isomorphic representation of the quantum canonical partition function. (42) Here we introduce the modifications necessary to construct an exact path integral representation for the canonical partition function of a multistate system using the mapping variables.

Consider the quantum mechanical partition function for a canonical ensemble,

$$Z = \text{Tr} \left[e^{-\beta \hat{H}} \right] = \sum_{n=1}^K \int d\mathbf{R} \langle \mathbf{R}, \psi_n | e^{-\beta \hat{H}} | \mathbf{R}, \psi_n \rangle, \quad 14.$$

where H is the diabatic Hamiltonian in Equation 10, $\beta = 1/k_B T$, $|\mathbf{R}\rangle$ represent nuclear position states, $|\psi_n\rangle$ are the diabatic electronic states. Inserting N copies of the identity operator,

$$\hat{\mathbb{I}} = \sum_{n=1}^K \int d\mathbf{R} |\mathbf{R}, \psi_n\rangle \langle \mathbf{R}, \psi_n|, \quad 15.$$

we obtain a product of high-temperature matrix elements in the electronic and nuclear degrees of freedom,

$$Z = \lim_{N \rightarrow \infty} \int d\mathbf{R}_1 \int d\mathbf{R}_2 \dots \int d\mathbf{R}_N \prod_{\alpha=1}^K \langle \mathbf{R}_\alpha | e^{-\beta_N H_0} | \mathbf{R}_{\alpha+1} \rangle \times I_{\text{el}}. \quad 16.$$

where $\beta_N = \beta/N$, the state-independent Hamiltonian, $H_0 = \frac{1}{2} \mathbf{P}^T \mathbf{M}^{-1} \mathbf{P} + V_0(\mathbf{R})$, and the electronic trace is defined as

$$I_{\text{el}} = \sum_{n_1} \sum_{n_2} \dots \sum_{n_N} \prod_{\alpha=1}^N \langle \psi_{n_\alpha} | e^{-\beta_N \mathbf{V}_e(\mathbf{R}_\alpha)} | \psi_{n_{\alpha+1}} \rangle. \quad 17.$$

Note that in Equations 16 and 17, the multistate ring polymer is cyclic with $\mathbf{R}_{N+1} = \mathbf{R}_1$, $\psi_{n_{N+1}} = \psi_{n_1}$. The high-temperature nuclear matrix elements can be evaluated within the Suzuki-Trotter approximation (75, 76) to obtain a nuclear phase space integral expression for the quantum canonical partition function,

$$Z \propto \lim_{N \rightarrow \infty} \int d\{\mathbf{R}, \mathbf{P}\} e^{-\beta_N H_{\text{rp}}(\{\mathbf{R}, \mathbf{P}\})} \times I_{\text{el}} \quad 18.$$

where we introduce the notation $\int d\{\mathbf{R}, \mathbf{P}\} \equiv \int d\mathbf{R}_1 \int d\mathbf{P}_1 \dots \int d\mathbf{R}_N \int d\mathbf{P}_N$ and the proportionality sign indicates that some constants have been omitted. The nuclear ring polymer Hamiltonian in Equation 18 is

$$H_{\text{rp}}(\{\mathbf{R}, \mathbf{P}\}) = \sum_{\alpha=1}^N \frac{1}{2} \mathbf{P}_\alpha^T \mathbf{M}^{-1} \mathbf{P}_\alpha + V_{\text{rp}}(\{\mathbf{R}\}), \quad 19.$$

with the ring polymer potential is defined as

$$V_{\text{rp}} = \sum_{\alpha=1}^N \frac{1}{2} \omega_N^2 (\mathbf{R}_\alpha - \mathbf{R}_{\alpha+1})^T \mathbf{M} (\mathbf{R}_\alpha - \mathbf{R}_{\alpha+1}) + V_0(\mathbf{R}_\alpha), \quad 20.$$

and $\omega_N = N/(\beta\hbar)$. The different multistate path integral based methods discussed in this review differ in their treatment of the electronic integral in Equation 17.

2.3.1. Mean-Field Formulation. The high-temperature electronic matrix elements in Equation 17

$$\langle \psi_n | e^{-\beta_N \mathbf{V}_e(\mathbf{R}_\alpha)} | \psi_m \rangle = [\mathbf{\Gamma}]_{nm}(\mathbf{R}_\alpha), \quad 21.$$

can be calculated either by diagonalizing the diabatic potential energy matrix when K is small, or analytically evaluated in the $N \rightarrow \infty$ limit (77),

$$[\mathbf{\Gamma}]_{nm}(\mathbf{R}) = \begin{cases} e^{-\beta_N V_{nn}(\mathbf{R})} & \text{if } n = m \\ (-\beta_N V_{nm}) e^{-\beta_N V_{nn}(\mathbf{R})} & \text{if } n \neq m \end{cases} \quad 22.$$

Substituting Equation 22 into Equations 17 and 18, we obtain an exact, mean-field path integral representation of the canonical partition function,

$$Z \propto \lim_{N \rightarrow \infty} \int d\{\mathbf{R}, \mathbf{P}\} e^{-\beta_N H_{\text{mf}}(\{\mathbf{R}\})} \text{sgn}(\Theta_{\text{mf}}), \quad 23.$$

where the Mean-Field Ring Polymer Hamiltonian is defined as,

$$H_{\text{mf}}(\{\mathbf{R}\}, \{\mathbf{P}\}) = \sum_{\alpha=1}^N \frac{1}{2} \mathbf{P}_{\alpha}^T \mathbf{M}^{-1} \mathbf{P}_{\alpha} + V_{\text{rp}}(\{\mathbf{R}\}) - \frac{1}{\beta_N} \ln(|\Theta_{\text{mf}}(\{\mathbf{R}\})|), \quad 24.$$

and the effective state-averaged potential is obtained from

$$\Theta_{\text{mf}} = \text{Tr} \left[\prod_{\alpha=1}^N \mathbf{\Gamma}(\mathbf{R}_{\alpha}) \right], \quad 25.$$

where the $K \times K$ matrix elements of $\mathbf{\Gamma}$ are as defined in Equation 22. Note that it is necessary to include the sign function in Equation 24 since Θ_{mf} is not necessarily positive for systems with $K > 2$.

In the Mean-Field framework, nuclei are time-evolved by integrating the classical equations of motion under the Mean-Field Hamiltonian in Equation 24,

$$\dot{\mathbf{R}}_{\alpha} = \frac{\partial H_{\text{mf}}}{\partial \mathbf{P}_{\alpha}} \quad \text{and} \quad \dot{\mathbf{P}}_{\alpha} = -\frac{\partial H_{\text{mf}}}{\partial \mathbf{R}_{\alpha}}, \quad 26.$$

These trajectories can then be used in a standard Path Integral Molecular Dynamics (PIMD) simulation (78) to calculate exact thermal equilibrium average properties for a multistate system.

2.3.2. Electronic Mapping Variable Path Integral. Deriving a classically isomorphic path integral expression for the electronic integral in Equation 17 using explicit mapping variables requires a new discretization protocol. Specifically, the discrete diabatic state identity operator in Equation 15 must be replaced with an identity defined in electronic position states (79),

$$\hat{1} = \int d\mathbf{x} |\mathbf{x}\rangle \langle \mathbf{x}| \hat{\mathcal{P}}, \quad 27.$$

where the projection operator, $\hat{\mathcal{P}}$, constrains the electronic mapping variables to the SEO basis,

$$\hat{\mathcal{P}} = \sum_{n=1}^K |n\rangle \langle n|. \quad 28.$$

Inserting N copies of this identity leads to an electronic integral of the form

$$I_{\text{el}} = \int d\mathbf{x}_1 \int d\mathbf{x}_2 \dots \int d\mathbf{x}_N \prod_{\alpha=1}^N \langle \mathbf{x}_{\alpha} | \hat{\mathcal{P}} e^{-\beta_N \mathbf{V}_e(\mathbf{R}_{\alpha})} \hat{\mathcal{P}} | \mathbf{x}_{\alpha+1} \rangle. \quad 29.$$

Using the definition of the SEO states and evaluating the matrix elements within the high-temperature Trotter approximation (80) yields an expression for the multistate partition function (79),

$$Z \propto \lim_{N \rightarrow \infty} \int d\{\mathbf{R}, \mathbf{P}\} \int d\{\mathbf{x}\} e^{-\beta_N H_{\text{rp}}} e^{-\sum_{\alpha=1}^N \mathbf{x}_{\alpha}^T \cdot \mathbf{x}_{\alpha}} \Theta_0(\{\mathbf{x}\}, \{\mathbf{R}\}). \quad 30.$$

In Equation 30, H_{rp} is previously defined in Equation 19, and the electron-nuclear coupling term is,

$$\Theta_0(\mathbf{x}, \mathbf{R}) = \text{Tr} \left[\prod_{\alpha=1}^N (\mathbf{x}_\alpha \otimes \mathbf{x}_\alpha^T) \Gamma(\mathbf{R}_\alpha) \right], \quad 31.$$

In Equation 31 we use the symbol \otimes to represent an outer product of the K -dimensional electronic position vectors. It is possible to compute exact, thermal equilibrium properties for K -level system using standard Path Integral Monte Carlo (PIMC) importance sampling (81).

Deriving a classically isomorphic representation for the canonical partition function requires that we arrive at an integral form in *phase space* for both the electronic and nuclear degrees of freedom. The next section discusses some of the different ways in which electronic phase space distributions can be generated.

2.4. Approximate real-time correlation functions

Kubo Transform Correlation Functions

Dynamical observables for systems in or near thermal equilibrium can frequently be obtained from real-time thermal correlation functions. In classical mechanics, correlation functions are obtained as a thermal ensemble average over the product of observable A at time $t = 0$ and observable B at time t . The corresponding quantum real-time thermal correlation function can take several forms, here we focus on the Kubo-transform correlation function (82, 83),

$$C_{AB}^{\text{kubo}}(t) = \frac{1}{\beta Z} \int_0^\beta d\lambda \text{Tr} \left[e^{-(\beta-\lambda)\hat{H}} \hat{A} e^{-\lambda\hat{H}} e^{i\hat{H}t/\hbar} \hat{B} e^{-i\hat{H}t/\hbar} \right], \quad 32.$$

that emerges naturally from linear response theory for the calculation of transport properties. The Kubo transform correlation function shares symmetries with the classical correlation function, and it can be shown that both RPMD (39) and MV-RPMD (50, 58) correlation functions take this form in the $t \rightarrow 0$ limit.

2.4.1. Ring Polymer Molecular Dynamics. For an adiabatic (single surface) process, there is no coupling between electronic and nuclear motion, and the path integral representation of the canonical partition function in Equation 18 simplifies to,

$$Z \propto \lim_{N \rightarrow \infty} \int d\{\mathbf{R}, \mathbf{P}\} e^{-\beta_N H_{\text{rp}}(\{\mathbf{R}, \mathbf{P}\})} \quad 33.$$

where the ring polymer Hamiltonian is previously defined in Equation 19. Molecular dynamics trajectories generated by this Hamiltonian,

$$\dot{\mathbf{R}}_\alpha = \frac{\partial H_{\text{rp}}}{\partial \mathbf{P}_\alpha} \quad \text{and} \quad \dot{\mathbf{P}}_\alpha = -\frac{\partial H_{\text{rp}}}{\partial \mathbf{R}_\alpha}, \quad 34.$$

sample the canonical ensemble and are used in standard Path Integral Molecular Dynamics (PIMD) simulations to compute exact thermal equilibrium average properties (78).

RPMD uses these same molecular dynamics trajectories to approximate the real-time Kubo-transform correlation function as,

$$C_{AB}^{\text{rp}} = \frac{1}{Z} \int d\{\mathbf{R}, \mathbf{P}\} e^{-\beta H_{\text{rp}}} \bar{A}(\{\mathbf{R}(\mathbf{0})\}, \{\mathbf{P}(\mathbf{0})\}) \bar{B}(\{\mathbf{R}(\mathbf{t})\}, \{\mathbf{P}(\mathbf{t})\}), \quad 35.$$

where $\bar{O} = \sum_{\alpha=1}^N O(\mathbf{P}_{\alpha}, \mathbf{R}_{\alpha})$ are the bead-averaged values of the corresponding operator, and the time-evolved positions and momenta are obtained by integrating the equations of motion in Equation 34

The RPMD approach offers some key advantages over other classical trajectory based approaches for condensed phase quantum dynamics. First, the dynamics, by construction, conserve the quantum Boltzmann distribution — this feature ensures that despite the use of classical trajectories RPMD simulations do not suffer from unphysical zero-point energy leakage, a common difficulty in semiclassical mapping variable methods (84, 85). Second, it has been shown that the Ring Polymer transition state as defined by RPMD rate theory emerges naturally as the $t \rightarrow 0+$ limit of the Generalized Kubo-transform flux-side correlation function (86, 87, 88). Finally, as reviewed elsewhere (41), RPMD and related methods have been remarkably successful in high-dimensional simulations of Born-Oppenheimer dynamics.

2.4.2. Mean-Field Ring Polymer Molecular Dynamics. As described in section 2.3.1, tracing over the electronic degrees of freedom yields a Mean-Field path integral expression in nuclear phase space. Mean-Field Ring Polymer Molecular Dynamics (MF-RPMD) (89), borrowing from the RPMD idea, approximates the real-time Kubo-transform correlation function for a multistate system as,

$$C_{AB}^{\text{mf}} = \frac{1}{Z} \int d\{\mathbf{R}, \mathbf{P}\} e^{-\beta H_{\text{mf}} \text{sgn}(\Theta_{\text{mf}})} \bar{A}(\{\mathbf{R}(\mathbf{0}), \mathbf{P}(\mathbf{0})\}) \bar{B}(\{\mathbf{R}(\mathbf{t}), \mathbf{P}(\mathbf{t})\}), \quad 36.$$

where \bar{O} indicates the bead-averaged function corresponding to operator \hat{O} , and the time-evolved positions and momenta are obtained by integrating the Mean-Field equations of motion defined in Equation 26.

In MF-RPMD, the nuclei evolve in time under an effective state-averaged electronic potential and the dynamics conserve the quantum Boltzmann distribution by construction. MF-RPMD is practical, easy to implement, and accurate in the strong to moderate coupling regimes but the lack of explicit electronic variables makes MF-RPMD inaccurate in nonadiabatic, weak-coupling regime.

2.4.3. Mapping Variable Ring Polymer Molecular Dynamics. The N integrals over electronic positions in Equation 29 can be rewritten as a trace over each of the N electronic variables (50). The trace over an operator can be written as a phase space integral over its Wigner function,

$$\text{Tr} \left[\hat{\mathcal{P}} e^{-\beta_N \mathbf{V}_e(\mathbf{R}_{\alpha})} \hat{\mathcal{P}} \right] = \int d\mathbf{x}_{\alpha} \int d\mathbf{p}_{\alpha} \int d\Delta\mathbf{x}_{\alpha} e^{i\mathbf{p}_{\alpha} \cdot \Delta\mathbf{x}_{\alpha}} \left\langle \mathbf{x}_{\alpha} + \frac{\Delta\mathbf{x}_{\alpha}}{2} \left| \hat{\mathcal{P}} e^{-\beta \mathbf{V}_e(\mathbf{R}_{\alpha})} \hat{\mathcal{P}} \right| \mathbf{x}_{\alpha} - \frac{\Delta\mathbf{x}_{\alpha}}{2} \right\rangle. \quad 37.$$

It is sufficient to include a single projection operator in Equation 37 is to constrain the electronic mapping variables to the SEO subspace, but inserting a pair of projection operators symmetrically about the potential operator enables analytic evaluation of the Wigner

transform. The resulting expression for the electronic integral is (50)

$$I_{\text{el}}(\{\mathbf{R}\}) = \int d\{\mathbf{x}, \mathbf{p}\} e^{-\sum_{\alpha=1}^N (\mathbf{x}_{\alpha} \cdot \mathbf{x}_{\alpha} + \mathbf{p}_{\alpha} \cdot \mathbf{p}_{\alpha})} \prod_{\alpha=1}^N \left(\mathbf{C}_{\alpha} - \frac{\mathbb{I}}{2} \right) \Gamma(\mathbf{R}_{\alpha}), \quad 38.$$

where \mathbb{I} is the $K \times K$ identity matrix, and the complex electronic matrix,

$$\mathbf{C}_{\alpha} = (\mathbf{x}_{\alpha} + i\mathbf{p}_{\alpha}) \otimes (\mathbf{x}_{\alpha} - i\mathbf{p}_{\alpha})^T. \quad 39.$$

Inserting the electronic integral back into the expression for canonical partition function in Equation 18 yields an exact, classically isomorphic, phase space integral in the nuclear degrees of freedom and the electronic mapping variables,

$$Z \propto \lim_{N \rightarrow \infty} \int d\{\mathbf{R}, \mathbf{P}\} \int d\{\mathbf{x}, \mathbf{p}\} e^{-\beta_N H_{\text{mv}}} e^{-\sum_{\alpha=1}^N (\mathbf{x}_{\alpha} \cdot \mathbf{x}_{\alpha} + \mathbf{p}_{\alpha} \cdot \mathbf{p}_{\alpha})} \text{sgn}(\Theta_{\text{mv}}), \quad 40.$$

where the mapping variable Hamiltonian,

$$H_{\text{mv}} = H_{\text{rp}}(\{\mathbf{R}, \mathbf{P}\}) - \frac{1}{\beta_N} \ln(|\Theta_{\text{mv}}|) \quad 41.$$

with the ring polymer Hamiltonian, H_{rp} , defined in Equation 19, and the interaction term,

$$\Theta_{\text{mv}} = \text{Re} \left(\text{Tr} \left[\prod_{\alpha=1}^N \left(\mathbf{C}_{\alpha} - \frac{\mathbb{I}}{2} \right) \Gamma(\mathbf{R}_{\alpha}) \right] \right). \quad 42.$$

Because Θ_{mv} is not necessarily positive, the absolute value is used in Equation 41 and the corresponding sign function is included in Equation 40; in Equation 42, the real part of the product of complex matrices, \mathbf{C}_{α} , is used since the canonical partition function and the Kubo-transform correlation function are real-valued.

The MV-RPMD approximation to the multistate Kubo-transform correlation functions can now be written as,

$$C_{AB}^{\text{mv}}(t) = \frac{1}{Z} \lim_{N \rightarrow \infty} \int d\{\mathbf{R}, \mathbf{P}\} \int d\{\mathbf{x}, \mathbf{p}\} e^{-\beta_N H_{\text{mv}}} e^{-\sum_{\alpha=1}^N (\mathbf{x}_{\alpha} \cdot \mathbf{x}_{\alpha} + \mathbf{p}_{\alpha} \cdot \mathbf{p}_{\alpha})} \text{sgn}(\Theta_{\text{mv}}) \bar{A}(\{\mathbf{R}, \mathbf{P}, \mathbf{x}, \mathbf{p}(0)\}) \bar{B}(\{\mathbf{R}, \mathbf{P}, \mathbf{x}, \mathbf{p}(t)\}), \quad 43.$$

where the time-evolved positions and momenta are generated by the mapping variable ring polymer Hamiltonian in Equation 41, and the bead-averaged functions, $\bar{A} = \sum_{\alpha=1}^N A(\mathbf{R}_{\alpha})$. The sign function, $\text{sgn}(\Theta_{\text{mv}})$, in Equation 43 and the exponential of $\sum_{\alpha=1}^N (\mathbf{x}_{\alpha} \cdot \mathbf{x}_{\alpha} + \mathbf{p}_{\alpha} \cdot \mathbf{p}_{\alpha})$ are constants of motion (50, 54) that weight the contribution of each trajectory at $t = 0$. Like RPMD, MV-RPMD trajectories conserve the Quantum Boltzmann distribution, and for dynamics on a single electronic surface the MV-RPMD Hamiltonian simplifies to the RPMD Hamiltonian.

2.4.4. Alternate Multistate Ring Polymer Molecular Dynamics Methods. Rather than the projected position space identity in Equation 27, it is possible to define an identity in momentum states, or even coherent states to arrive at different but formally exact, classically isomorphic representations of the canonical partition function. The alternate multistate RPMD methods for approximate dynamics differ both in the formulation of the

initial thermal distribution and the Hamiltonian used to generate trajectories in real time.

Nonadiabatic Ring Polymer Molecular Dynamics (NRPMD). Path integral discretization of the Boltzmann operator in electronic variables can be performed by introducing $N/2$ copies of the projected position space identity in Equation 27 and $N/2$ copies of a projected momentum space identity. Analytic evaluation of the resulting electronic matrix elements yields an exact, phase-space expression for the canonical partition function (55),

$$Z \propto \lim_{N \rightarrow \infty} \int d\{\mathbf{R}, \mathbf{P}\} \int d\{\mathbf{x}, \mathbf{p}\} e^{-\beta N H_{\text{rp}}} e^{-\left(\sum_{\alpha=1}^N \mathbf{x}_{\alpha} \cdot \mathbf{x}_{\alpha} + \mathbf{p}_{\alpha} \cdot \mathbf{p}_{\alpha}\right)} \Theta_{\text{nr}}, \quad 44.$$

where

$$\Theta_{\text{nr}} = \text{Tr} \left[\prod_{\alpha=1}^N \left(\mathbf{p}_{\alpha-1}^T \boldsymbol{\Gamma}(R_{\alpha}) \mathbf{x}_{\alpha} \right) \left(\mathbf{x}_{\alpha}^T \boldsymbol{\Gamma}(R_{\alpha}) \mathbf{p}_{\alpha} \right) \right], \quad 45.$$

where the matrix $\boldsymbol{\Gamma}$ is defined in Equation 21.

The proposed NRPMD approximation to the Kubo-transform correlation function is (55),

$$C_{AB}^{\text{nr}}(t) = \frac{1}{Z} \lim_{N \rightarrow \infty} \int d\{\mathbf{R}, \mathbf{P}\} \int d\{\mathbf{x}, \mathbf{p}\} e^{-\beta N H_{\text{rp}}} e^{-\left(\sum_{\alpha=1}^N \mathbf{x}_{\alpha} \cdot \mathbf{x}_{\alpha} + \mathbf{p}_{\alpha} \cdot \mathbf{p}_{\alpha}\right)} \Theta_{\text{nr}} \bar{A}(\{\mathbf{R}, \mathbf{P}, \mathbf{x}, \mathbf{p}(0)\}) \bar{B}(\{\mathbf{R}, \mathbf{P}, \mathbf{x}, \mathbf{p}(t)\}), \quad 46.$$

where \bar{A} and \bar{B} are bead-averaged functions, and the time-evolved positions and momenta are obtained by integrating equations of motion generated by a different Hamiltonian,

$$H_{\text{nr}} = H_{\text{rp}}(\{R, P\}) + \frac{1}{2} \sum_{\alpha=1}^N \left(\mathbf{x}_{\alpha}^T \mathbf{V}_e \mathbf{x}_{\alpha} + \mathbf{p}_{\alpha}^T \mathbf{V}_e \mathbf{p}_{\alpha} - \text{Tr}[\mathbf{V}_e] \right). \quad 47.$$

It is clear that equations of motion for the electronic mapping variables under the NRPMD Hamiltonian in Equation 47 describe each bead evolving under the semiclassical MMST Hamiltonian previously defined in Equation 12. However, unlike RPMD, MF-RPMD, and MV-RPMD, the classical trajectory ensemble used here does not conserve the Quantum Boltzmann distribution.

Coherent State Ring Polymer Molecular Dynamics (CS-RPMD). As the name suggests, CS-RPMD is derived by inserting identity in the form of an overcomplete set of coherent states (59). Evaluating the electronic integral then yields an expression that is exact in the $N \rightarrow \infty$ limit,

$$Z \propto \lim_{N \rightarrow \infty} \int d\{\mathbf{R}, \mathbf{P}\} \int d\{\mathbf{x}, \mathbf{p}\} e^{-\beta N H_{\text{cs}}} \Theta_{\text{cs}}, \quad 48.$$

where the CS-RPMD Hamiltonian is,

$$H_{\text{cs}} = H_{\text{rp}} + \sum_{\alpha=1}^N \frac{1}{2} \left(\mathbf{x}_{\alpha}^T \mathbf{V}_e \mathbf{x}_{\alpha} + \mathbf{p}_{\alpha}^T \mathbf{V}_e \mathbf{p}_{\alpha} \right) - \text{Tr}[\mathbf{V}_e] \quad 49.$$

with the interaction term,

$$\Theta_{\text{cs}} = e^{-\sum_{\alpha} (\mathbf{x}_{\alpha} \cdot \mathbf{x}_{\alpha} + \mathbf{p}_{\alpha} \cdot \mathbf{p}_{\alpha})} \text{Tr} \left[\prod_{\alpha=1}^N \frac{1}{2} (\mathbf{x}_{\alpha} + \mathbf{p}_{\alpha}) \otimes (\mathbf{x}_{\alpha} - i\mathbf{p}_{\alpha})^T \right]. \quad 50.$$

CS-RPMD approximates the Kubo-transform correlation function as,

$$C_{AB}^{cs}(t) = \frac{1}{Z} \int d\{\mathbf{R}, \mathbf{P}\} \int d\{\mathbf{x}, \mathbf{p}\} e^{-\beta_N H_{cs}} \Theta_{cs} \bar{A}(\{\mathbf{R}, \mathbf{P}, \mathbf{x}, \mathbf{p}(0)\}) \bar{B}(\{\mathbf{R}, \mathbf{P}, \mathbf{x}, \mathbf{p}(t)\}), \quad 51.$$

where the time-evolved positions and momenta are generated by the CS-RPMD Hamiltonian in Equation 49. Unfortunately, CS-RPMD trajectories also fail to conserve the Quantum Boltzmann distribution since Θ_{cs} is not a constant of motion.

Summarizing the features of MV-RPMD, NRPMD, and CS-RPMD

At $t = 0$ the MV-RPMD correlation functions is the exact Kubo transform correlation function for linear operators. In the adiabatic limit where nuclear dynamics occurs on a single electronic surface, all three approximations reduce to RPMD. And finally, integrating out the electronic variables analytically in all three cases yields MF-RPMD (79).

The MV-RPMD Hamiltonian generates an ensemble of classical trajectories that conserve the quantum Boltzmann distribution (50, 54). The trajectories generated by the MMST-like Hamiltonians in NRPMD and CS-RPMD, like nonadiabatic LSC-IVR (19), fail to conserve the quantum Boltzmann distribution. This failure can lead to zero-point energy leakage, and an ‘inverted potential’ problem where the electronic potential takes on negative values (? ? 84).

For a bare two-level system with no coupled nuclear degrees of freedom, MV-RPMD fails to capture Rabi oscillations. As one might expect from the success of LSC-IVR for bare two-level systems (19, 79), both NRPMD and CS-RPMD do successfully capture Rabi oscillations (55, 59). In the limiting case of a single ring polymer bead, $N = 1$, the MV-RPMD and NRPMD Hamiltonians are identical, and like CS-RPMD capture Rabi oscillations and conserve the *classical* MMST Boltzmann distribution.

2.5. Exact Quantum Liouvillian in the Mapping Variable Representation

Deriving an exact ring polymer Liouvillian for quantum dynamics in the mapping variable framework is a step towards the rigorous derivation of approximate, real-time, multistate RPMD methods. For adiabatic dynamics, it has been shown that RPMD and CMD can both be connected to an exact quantum Liouvillian derived from a Generalized Kubo transform correlation function that is equivalent to the Kubo transform correlation function for bead-invariant operators and in the $N \rightarrow \infty$ limit (86, 87, 90).

An analytic expression for the exact N -beath path integral Liouvillian in the phase space of the nuclear and electronic degrees of freedom can be similarly derived (91),

$$\mathcal{L}^{[N]} = \mathcal{L}_{\text{nuc}}^{[N]} + \mathcal{L}_{\text{elec}}^{[N]} + \mathcal{L}_{\text{hd}}^{[N]}, \quad 52.$$

where the first term corresponds to nuclear evolution on an Ehrenfest-like average electronic surface,

$$\mathcal{L}_{\text{nuc}}^{[N]} = \sum_{\alpha=1}^N \mathbf{P}_{\alpha}^T \mathbf{M}^{-1} \frac{\partial}{\partial \mathbf{R}_{\alpha}} - \frac{2}{\hbar} [V_0(\mathbf{R}_{\alpha}) + V_{\text{sc}}(\mathbf{R}_{\alpha}, x_{\alpha}, \mathbf{p}_{\alpha})] \sin \left(\frac{\hbar}{2} \overleftarrow{\frac{\partial}{\partial \mathbf{R}_{\alpha}}} \overrightarrow{\frac{\partial}{\partial \mathbf{P}_{\alpha}}} \right), \quad 53.$$

the second term describes the Rabi oscillations of the electronic degrees of freedom along with higher order couplings to nuclear derivatives,

$$\mathcal{L}_{\text{elec}}^{[N]} = \sum_{\alpha=1}^N \frac{1}{\hbar} \left[\mathbf{p}_\alpha \mathbf{V}_e(\mathbf{R}_\alpha) \overrightarrow{\nabla_{\mathbf{x}_\alpha}} - \mathbf{x}_\alpha \mathbf{V}_e(\mathbf{R}_\alpha) \overrightarrow{\nabla_{\mathbf{p}_\alpha}} \right] \cos \left(\frac{\hbar}{2} \overleftarrow{\frac{\partial}{\partial \mathbf{R}_\alpha}} \overrightarrow{\frac{\partial}{\partial \mathbf{P}_\alpha}} \right), \quad 54.$$

and the third terms corresponds to nuclear and electronic evolution due to higher-order derivatives in both degrees of freedom,

$$\mathcal{L}_{\text{hd}}^{[N]} = \sum_{\alpha=1}^N \frac{1}{4} \left[\overrightarrow{\nabla_{\mathbf{x}_\alpha}} \mathbf{V}_e(\mathbf{R}_\alpha) \overrightarrow{\nabla_{\mathbf{x}_\alpha}} + \overrightarrow{\nabla_{\mathbf{p}_\alpha}} \mathbf{V}_e(\mathbf{R}_\alpha) \overrightarrow{\nabla_{\mathbf{p}_\alpha}} \right] \sin \left(\frac{\hbar}{2} \overleftarrow{\frac{\partial}{\partial \mathbf{R}_\alpha}} \overrightarrow{\frac{\partial}{\partial \mathbf{P}_\alpha}} \right). \quad 55.$$

In Equation 53, V_{sc} is the MMST potential (last term in Equation 12) and the arrows over the F -dimensional nuclear partial derivatives indicates the direction in which the derivative is evaluated. In Equation 54, \mathbf{V}_e is the diabatic potential energy matrix and $\nabla_{\mathbf{x}/\mathbf{p}}$ indicate partial derivatives with respect to the K -dimensional vectors of electronic position/momentum mapping variables respectively.

Interestingly, all three terms in the Liouvillian describe a ring polymer dynamics where each bead evolves *independently* in time. The beads are however connected to each other at time $t = 0$ through the initial thermal distribution that resembles the MV-RPMD distribution for the electron degrees of freedom, but includes an additional non-trivial Wigner transform in the nuclear degrees of freedom (91). Constructing an approximate classical ring polymer Hamiltonian for multistate system dynamics requires that the exact quantum Liouvillian be truncated to eliminate higher order derivatives.

Truncating $\mathcal{L}^{[N]}$ to $\mathcal{O}(\hbar^0)$ results in classical dynamics that do not conserve the quantum Boltzmann distribution,

$$\mathcal{L}_0^{[N]} = \sum_{\alpha=1}^N \mathbf{P}_\alpha^T \mathbf{M}^{-1} \frac{\partial}{\partial \mathbf{R}_\alpha} - [V_0(\mathbf{R}_\alpha) + V_{\text{sc}}(\mathbf{R}_\alpha, x_\alpha, \mathbf{p}_\alpha)] \overleftarrow{\frac{\partial}{\partial \mathbf{R}_\alpha}} \overrightarrow{\frac{\partial}{\partial \mathbf{P}_\alpha}} \quad 56.$$

$$+ \frac{1}{\hbar} \left[\mathbf{p}_\alpha \mathbf{V}_e(\mathbf{R}_\alpha) \overrightarrow{\nabla_{\mathbf{x}_\alpha}} - \mathbf{x}_\alpha \mathbf{V}_e(\mathbf{R}_\alpha) \overrightarrow{\nabla_{\mathbf{p}_\alpha}} \right]. \quad 57.$$

This truncated Liouvillian corresponds to time evolution of the electronic mapping variables under the NRPMD Hamiltonian in Equation 47 although trajectory initial conditions are drawn from a different thermal distribution.

2.5.1. Matsubara approximation. A complex Matsubara Liouvillian for adiabatic dynamics can be derived by re-writing the exact ring polymer Liouvillian in terms of the N normal modes of a free ring polymer and then truncating to include only $M < N$ ‘smooth’ or Matsubara modes (86). The resulting complex Liouvillian preserves the quantum Boltzmann distribution, and the real part describes dynamics under the RPMD Hamiltonian (86, 87, 90, 92).

Similarly, starting with the exact, multistate ring polymer Liouvillian (91), transforming to the normal modes of the free nuclear ring polymer and truncating to include only $M < N$ normal modes yields a complex multistate ‘Matsubara’ Liouvillian (58). Unlike the adiabatic case, this multistate Liouvillian does not conserve the quantum Boltzmann distribution for a general K -level system. Taking the real part of this multistate Matsubara Liouvillian suggest a new approximation for the Kubo transform correlation function that is

a hybrid of MV-RPMD and NRPMD. Specifically, a dynamics where the initial conditions are drawn from the MV-RPMD distribution and real-time trajectories are generated from the NRPMD Hamiltonian (58).

3. Implementation

All calculations using the imaginary-time path integral based methods discussed here are converged in the limit $N \rightarrow \infty$. It is expected that multistate RPMD methods will converge with relatively low N values for nonadiabatic system simulations since the number of beads depends on temperature and the magnitude of the electronic coupling.

3.1. Thermal Correlation Functions

Approximate multistate RPMD thermal correlation functions take the form,

$$C_{AB}^{ms}(t) = \frac{\langle A(\{\mathbf{x}_0, \mathbf{p}_0, \mathbf{R}_0, \mathbf{P}_0\}) B(\{\mathbf{x}_t, \mathbf{p}_t, \mathbf{R}_t, \mathbf{P}_t\}) Q(\{\mathbf{x}_0, \mathbf{p}_0, \mathbf{R}_0, \mathbf{P}_0\}) \rangle_W}{\langle Q(\{\mathbf{x}_0, \mathbf{p}_0, \mathbf{R}_0, \mathbf{P}_0\}) \rangle_W}, \quad 58.$$

where $ms = \{mv, nr, cs\}$, the subscripts 0 and t indicate the initial and time-evolved phase space vectors respectively, and we use the notation $\langle \cdot \rangle_W$ to indicate a thermal ensemble average over a distribution W . Trajectory initial conditions are generated from the distribution W using standard PIMC or PIMD methods, and then time-evolved by integrating Hamilton's equation of motion for a multistate Hamiltonian,

$$\dot{\mathbf{x}}_\alpha = \frac{\partial H_{ms}}{\partial \mathbf{p}_\alpha} \quad \dot{\mathbf{p}}_\alpha = -\frac{\partial H_{ms}}{\partial \mathbf{x}_\alpha} \quad 59.$$

$$\dot{\mathbf{R}}_\alpha = \frac{\partial H_{ms}}{\partial \mathbf{P}_\alpha} \quad \dot{\mathbf{P}}_\alpha = -\frac{\partial H_{ms}}{\partial \mathbf{R}_\alpha}. \quad 60.$$

The specific form of the distribution, W , and the multistate Hamiltonian, H_{ms} , for real-time dynamics for each of the approximate multistate RPMD methods described here is specified in **Table 1**.

The function Q that appears in the denominator of Equation 58 is the estimator for the canonical partition function such that,

$$Z = \lim_{N \rightarrow \infty} \int d\{\mathbf{R}, \mathbf{P}\} \int d\{\mathbf{x}, \mathbf{p}\} Q(\mathbf{x}, \mathbf{p}, \mathbf{R}, \mathbf{P}) W(\mathbf{x}, \mathbf{p}, \mathbf{R}, \mathbf{P}). \quad 61.$$

For single surface Born-Oppenheimer processes, $Q = 1$ but for multistate systems this function accounts for the fact that the isomorphic classical expression for the canonical partition function does not, in general, correspond to a positive definite distribution.

3.2. Estimators

The functions A and B in the numerator of Equation 58 are estimators derived to yield the exact thermal equilibrium average values, $\langle \hat{A} \rangle$ and $\langle \hat{B} \rangle$, when the trajectory ensemble is sampled from the function W . We will not present detailed derivations here, but simply introduce some of the estimators most frequently used in the multistate RPMD methods.

When the operators depend on nuclear position, $O(\hat{\mathbf{R}})$, the corresponding bead-averaged estimators are $O(\{\mathbf{R}\}) = 1/N \sum_{\alpha=1}^N O(\mathbf{R}_\alpha)$. For electronic state population operators, several estimators have been derived and shown to be exact for the calculation of thermal

Table 1 Implementation details for MV-RPMD, NRPMD, and CS-RPMD

Method	W	Sampling	Q	H_{ms}
MV-RPMD	$e^{-\beta H_{\text{mv}}} e^{-\sum_{\alpha=1}^N (\mathbf{x}_{\alpha} \cdot \mathbf{x}_{\alpha} + \mathbf{p}_{\alpha} \cdot \mathbf{p}_{\alpha})}$	PIMC	$\text{sgn}(\Theta_{\text{mv}})$ ^a	H_{mv} ^b
NRPMD	$e^{-\beta H_{\text{rp}}} e^{-\sum_{\alpha=1}^N (\mathbf{x}_{\alpha} \cdot \mathbf{x}_{\alpha} + \mathbf{p}_{\alpha} \cdot \mathbf{p}_{\alpha})} \Theta_{\text{nr}} $	PIMC	$\text{sgn}(\Theta_{\text{nr}})$ ^c	H_{nr} ^d
CS-RPMD	$e^{-\beta H_{\text{cs}}}$	PIMD	Θ_{cs} ^e	H_{cs} ^f
Hybrid MS-RPMD ^g	$e^{-\beta H_{\text{mv}}} e^{-\sum_{\alpha=1}^N (\mathbf{x}_{\alpha} \cdot \mathbf{x}_{\alpha} + \mathbf{p}_{\alpha} \cdot \mathbf{p}_{\alpha})}$	PIMC	$\text{sgn}(\Theta_{\text{mv}})$	H_{nr}

^a Equation 42; ^b Equation 41 ^c Equation 45; ^d Equation 47 ^e Equation 50; ^f Equation 49 ^g Hybrid multistate RPMD from nonadiabatic Matsubara derivation (58)

equilibrium properties. Specifically, three estimators have been derived for the electronic state projection operator, $\mathcal{P}_n = |n\rangle\langle n|$, in the MV-RPMD framework. The ‘Boltzmann’ population estimator takes the form (50),

$$\mathcal{P}_n^{\beta} = \frac{[\Theta_{\text{mv}}]_{nn}}{\text{Tr}[\Theta_{\text{mv}}]}, \quad 62.$$

where the matrix Θ_{mv} is defined in Equation 42 and we use the notation $[\cdot]_{nn}$ to indicate the corresponding matrix element. The ‘Wigner’ estimator has been used in the simulation of photo-initiated excited state dynamics (51),

$$\mathcal{P}_n^{\text{W}} = \frac{2^{K+1}}{N} \sum_{\alpha=1}^N e^{-\sum_{\alpha} \mathbf{x}_{\alpha} \cdot \mathbf{x}_{\alpha} + \mathbf{p}_{\alpha} \cdot \mathbf{p}_{\alpha}} \left([\mathbf{x}_{\alpha}]_n^2 + [\mathbf{p}_{\alpha}]_n^2 - \frac{\hbar}{2} \right). \quad 63.$$

The ‘semiclassical’ estimator was first introduced as a population estimator in NRPMD framework, but subsequently shown to be exact in the MV-RPMD framework as well (55, 52),

$$\mathcal{P}_n^{\text{sc}} = \frac{1}{2N} \sum_{\alpha=1}^N ([\mathbf{x}_{\alpha}]_n^2 + [\mathbf{p}_{\alpha}]_n^2 - \hbar). \quad 64.$$

Finally, in the CS-RPMD framework, the population estimator takes the form

$$\mathcal{P}_n^{\text{cs}} = \frac{1}{N} \sum_{\alpha=1}^N \frac{[\mathbf{x}_{\alpha} - i\mathbf{p}_{\alpha}]_n [\mathbf{x}_{\alpha+1} + i\mathbf{p}_{\alpha+1}]_n}{(\mathbf{x}_{\alpha} - i\mathbf{p}_{\alpha})^T (\mathbf{x}_{\alpha+1} + i\mathbf{p}_{\alpha+1})} \quad 65.$$

3.3. Nonequilibrium Correlation Functions

The short-time accuracy of RPMD for nonequilibrium correlation functions has been established through connections with Matsubara dynamics and demonstrated through numerical simulations (93). While the short-time accuracy of the multistate RPMD methods has not been clearly established, recent work developing a nonadiabatic Matsubara dynamics suggests that their performance is likely similar for thermal equilibrium correlation function and nonequilibrium correlation functions (58).

The protocol for initializing to a photo-induced excited state was developed in the context of the MV-RPMD framework (51), and later adapted to an NRPMD implementations as well (59). Assuming vertical Franck-Condon excitation, nuclear phase space variables can be initialized from a ground state equilibrium distribution. Initial conditions for electronic mapping variables are then chosen such that only one electronic state is initially populated.

Drawing on ideas from the semiclassical literature (94), this can be achieved by setting the Wigner or the Semiclassical population estimators (Equations 63 and 64) for *each* bead to be 0 for an unpopulated state, 1 for a fully populated state, or a number between 0 and 1 for partially populated states.

As a final note, it is necessary to determine a ‘dynamical temperature’ since the multi-state RPMD Hamiltonian depends on the inverse temperature, $\beta = 1/k_B T$. For a thermal simulation, β is determined by the physical temperature of the simulation. However, for a system initially in the excited state, in addition to correctly initializing the electronic mapping variables it is necessary to choose a fictitious dynamical temperature, T_d , to account for the excess energy introduced to the system upon photo-excitation. Numerical simulations demonstrate that the best choice of fictitious temperature is $T_d k_B = E_i$, where k_B is the Boltzmann constant and E_i is the total initial energy of the system (51).

4. Applications

Multistate RPMD methods have been used in a range of applications including vibronic spectra calculations (56), dynamic simulations of spin-boson models (55, 59, 50, 54), photoinduced excited state dynamics (51, 57), and in studies of proton-coupled electron transfer (52). In this section we discuss three specific studies that highlight the strengths of these approaches.

4.1. Two-level systems

Approximate multistate RPMD methods are benchmarked through the study of two-level systems coupled to a single nuclear degree of freedom. Nuclear dynamics is characterized through calculations of the nuclear position autocorrelation function where $\hat{A} = \hat{B} = \hat{\mathbf{R}}$.

In the adiabatic (strong coupling) regime, both the MF-RPMD and MV-RPMD nuclear autocorrelation functions agree well with exact quantum results, as shown in **Figure 1a**. As the coupling strength is decreased and nonadiabatic effects start to play a significant role MV-RPMD significantly outperforms MF-RPMD as shown in **Figures 1b-d**. While not shown here, it has been established that despite minor differences in the nuclear autocorrelation function calculated using MV-RPMD, CS-RPMD and NRPMD for these systems, there is little to choose between them in terms of accuracy (59). Further, a recent study of the use of mixed time-slicing (96) with MV-RPMD where different numbers of beads are used to describe the electronic and nuclear degrees of freedom suggests that when nuclear and electronic motion are strongly coupled, the best results are obtained by quantizing them to the same extent as demonstrated in **Figures 1e-f** (54).

Both NRPMD and CS-RPMD have been used to compute electronic state population correlation functions for these same model systems and find good agreement with exact quantum results (59, 57). Expectedly, these results closely resemble those generated by LSC-IVR calculations where the Wigner transform of the Boltzmann operator is obtained from an exact calculation (79). However, MV-RPMD population autocorrelation functions are noisy and deviate rapidly from the exact result even at relatively short times.

4.2. Excited State Dynamics

The different mechanisms of ultrafast photo-induced dissociation can be modeled using a manifold of three coupled excited states, where one is initially occupied through photo-

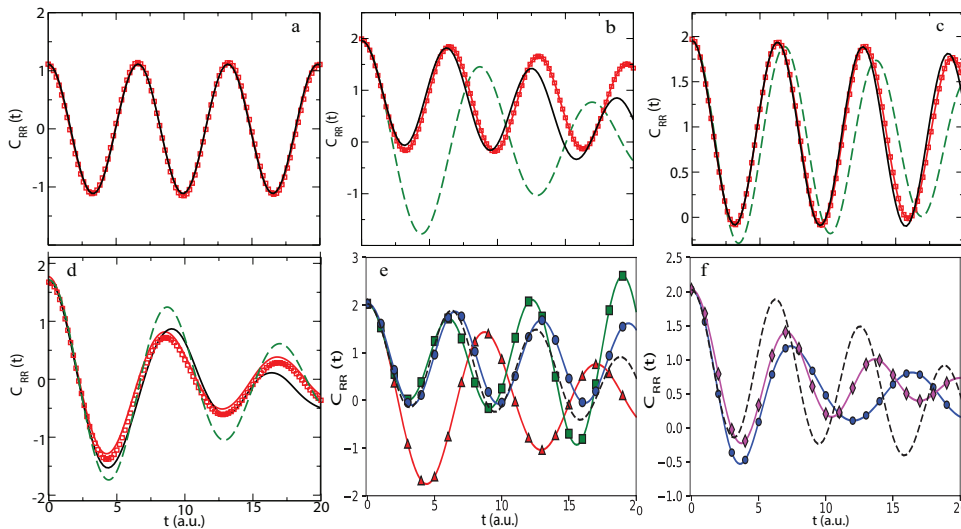


Figure 1

The MV-RPMD nuclear autocorrelation functions for a two-level system coupled to a single nuclear mode are calculated using Equation 43 with $A = B = \bar{R}$. The converged number of beads range from $N = 5$ in the weak and moderate coupling regimes to $N = 10$ in the strong coupling case. The number of trajectories required goes from 10^4 to 10^5 with the larger number corresponding to stronger coupling and more beads. The diagonal elements of the diabatic potential energy matrix are shifted oscillators, and the off-diagonal coupling is tuned from (a) the adiabatic, strong-coupling regime to (b) moderate coupling to (c) the nonadiabatic, weak-coupling regime with non-zero driving force and (d) a symmetric nonadiabatic coupling model. MV-RPMD results are plotted using red lines with squares and MF-RPMD results are shown in green dashed lines. Exact quantum results, generated by diagonalizing a DVR Hamiltonian on a grid (95), are shown with solid black lines. Figures adapted from reference (50). Figures (e) and (f) explore mixed time-slicing for the model system in (d) where different numbers of beads are used to discretize the electronic N_e and nuclear degrees of freedom N_n . (e) plots the nuclear position autocorrelation function with $N_e : N_n$ values 1 : 6 with red triangles, 3 : 6 with green squares, 6 : 6 with blue circles, and exact results with black dashed lines. (f) plots the nuclear autocorrelation function with more beads for the electronic state variable, 4 : 1 with magenta diamonds. Figures adapted from reference (54).

excitation. This study considers three model systems that differ in the relative timescales on which branching events are observed and in the extent of coupling between the different excited state surfaces (97).

Figure 2 panel (a) demonstrates that the time-dependent electronic state populations calculated in an MV-RPMD simulation capture the short-time behavior for all three model systems. However, at longer times, MV-RPMD proves less accurate particularly for the first model (top row), where the two curve crossing events are well separated in time. Results for the same models from an NRPMD simulation are shown in **Figure 2** panel (b). It is evident that these dynamics are more accurate at longer times, in particular even capturing the longer timescale transitions in the first model system. Interestingly, MV-RPMD simulations in the classical 1-bead limit are almost as accurate as NRPMD, as shown in **Figure 2** panel (c), likely because the MV-RPMD Hamiltonian reduces to the NRPMD Hamiltonian exactly in this limit.

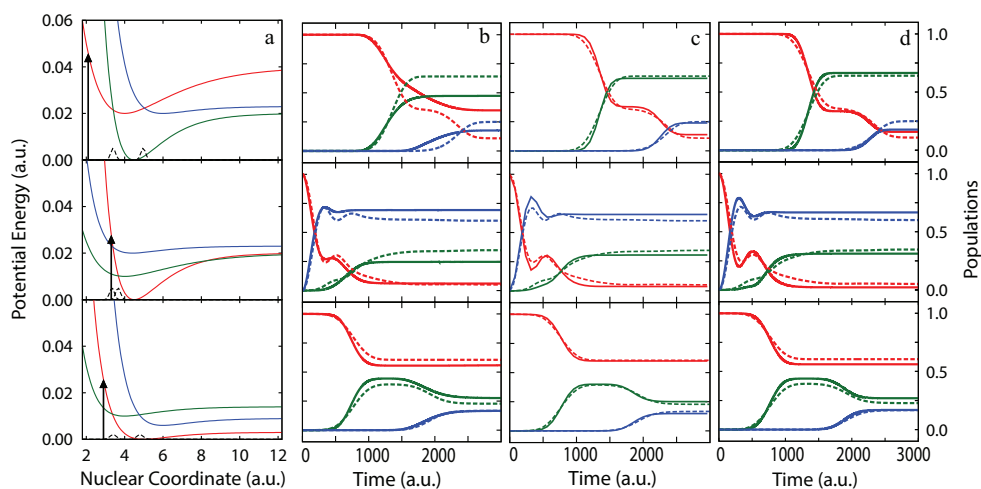


Figure 2

Vertical panel (a) shows three model systems where the three coupled excited state potential energy surfaces are described by Morse functions and the black arrow indicates the state initially populated upon photo-excitation from the ground state. (b) Excited state population dynamics from bead-converged ($N = 4$) MV-RPMD calculations using the Wigner estimator and are plotted in solid lines. The number of trajectories employed ranges from 2×10^3 to 3×10^4 with model I (top) requiring the fewest trajectories and model III (bottom) requiring the most. (c) Time-dependent populations from NRPMD using the semiclassical estimator are plotted using solid lines. Exact quantum results are plotted with dashed lines in both panels (b) and (c). Panel (d) shows MV-RPMD population dynamics in $N = 1$ classical limit that agree remarkably well with NRPMD results. Panels (a),(b), and (d) are adapted from Reference (51), and the plots in Panel (c) are made with data provided by the Authors of Reference (57).

4.3. Mechanistic study of Proton-Coupled Electron Transfer

Proton coupled electron transfer (PCET) reactions are a class of reactions that are central to understanding important chemical processes such as water-splitting catalysis, bio-inorganic reactions, and enzyme catalysis. PCET can be theoretically described using a system-bath model (2), where four electron-proton diabatic states are coupled to solvent degrees of freedom that are, in turn, coupled to a thermal bath representing the environment. The four electron-proton states are quasi-diabatic states labeled {DD, DA, AD, AA} where the first/second letters indicate the electron/proton is in its donor(D) or acceptor(A) state respectively. The mechanistic study described here focuses on the chronology of charged particle transfer—some systems exhibit concerted electron and proton transfer where others undergo sequential transfer events with either the electron transferring first (ET-PT mechanism) or the proton transferring first (PT-ET mechanism) (2).

MV-RPMD simulations were recently used to successfully characterize the mechanism of PCET in a series of model systems (52). A nonequilibrium initial distribution was generated by constraining the system to a dividing surface defined by nuclear configurations corresponding to the curve crossing between the reactant (DD) diabatic state and one of the other three diabatic states. Time-evolving trajectories forward and backward in time from this dividing surface served to highlight the different PCET mechanisms. Specifically, following the timescales on which population transferred from the reactant to the other diabatic states, yielded mechanistic insight. For instance, **Figure 3** shows the results of

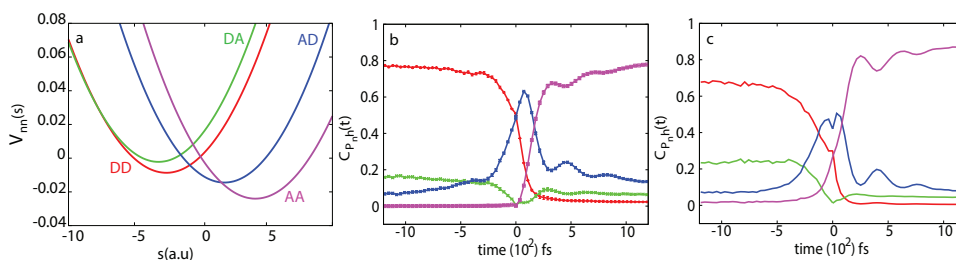


Figure 3

The four diabatic states, DD, DA, AD, AA for a model PCET system are pictured in figure (a). Figure (b) shows the change in population of each of the four diabatic states – color coded to match (a) – when an MV-RPMD simulation is initialized to nuclear configurations corresponding to the crossing of the DD and AD state; Using the focusing protocol introduced earlier, electronic mapping variables are initialized to ensure that the population of the DD and AD states are set equal to 0.5, with the populations of the DA and AA states set to zero. The population dynamics demonstrate that the PCET mechanism in this case is sequential with electron transfer preceding proton transfer (ET-PT). Figure (c) shows the population dynamics for this same model system where MV-RPMD trajectories are initialized to nuclear configurations corresponding to the crossing of the DD and AA state; electronic mapping variables are initialized to ensure that the population of the DD and AA states are set equal to 0.5, with the populations of the DA and AD states set to zero. The resulting population dynamics demonstrate that MV-RPMD correctly identifies the ET-PT mechanism independent of the choice of initial conditions. Calculations are converged with $N = 10$ beads using an ensemble of 10^5 classical trajectories.

an MV-RPMD study of populations dynamics for a model system initially constrained to an arbitrarily chosen dividing surfaces. The results from two different dividing surfaces are shown, and in both cases it is evident that as the population of the reactant state (DD) decreases, the population of the electron transfer (AD) state increases first, followed by a subsequent transfer of population from this state to the product state (AA). These studies served as the first demonstration of the utility of multistate RPMD methods in high-dimensional condensed phase systems, and further serves to establish dividing surface independence in MV-RPMD simulations of population dynamics (52).

5. Limitations

5.1. Reaction Rate Theory

The success of RPMD in the calculation of condensed phase reaction rates has been shown to arise from the connections between RPMD rate theory and the Quantum Transition State theory derived from the generalized Flux-side Kubo-transform correlation function (90). The development of a multistate RPMD rate theory is key to enabling large scale application of these methods and remains an outstanding challenge.

Other multistate methods based on RPMD have had some success in the calculation of rates, like Ring Polymer Surface Hopping (98), Kinetically Constrained (KC)-RPMD (99, 100), and MF-RPMD for the calculation of adiabatic and nonadiabatic reaction rates in multistate systems (101). KC-RPMD introduces a single auxiliary variable that reports on the probability of electronic transitions and employs trajectories that conserve an approximate quantum Boltzmann distribution in this expanded phase space (99). Nonadiabatic reaction rates calculated in the MF-RPMD framework require the introduction of an *ad hoc* constraint to ensure that trajectories pass through the electronic transition

state (101). In a practical sense, MF-RPMD offers a simple and scalable approach to the calculation of nonadiabatic condensed phase reaction rates, however, the lack of explicit electronic variables limits mechanistic insights.

Given the importance of dynamics that preserve detailed balance in the context of rate calculations, we expect that recent work understanding the nature of MV-RPMD dynamics (91, 53, 54), and the derivation of new population estimators (51, 52) will pave the way to developing a rigorous rate theory with explicit electronic variables.

5.2. Detailed Balance and Rabi Oscillations

As discussed in earlier sections, multistate RPMD methods developed to date either conserve the quantum Boltzmann distribution (MV-RPMD) or correctly describe the electronic transitions in a bare two-level systems (NRPMD, CS-RPMD). The hybrid multistate method derived from the nonadiabatic Matsubara Liouvillian also falls in this latter category, with dynamics that do not obey detailed balance. Deriving an imaginary-time path integral based dynamics that can both capture Rabi oscillations and preserve detailed balance remains an outstanding theoretical challenge in the development.

5.3. Ab-initio Path Integrals for Nonadiabatic Dynamics

Ab-initio dynamics refers to trajectory based simulations where the potential energy and forces are computed from electronic structure on-the-fly. Ab-initio multistate path integral dynamics face a couple of additional challenges. First, it is necessary to solve the Schrödinger equation for multiple adiabatic eigenvalues and eigenstates at each time step. Second, the multistate methods described here all assume a diabatic electronic Hamiltonian whose diagonal and off-diagonal elements must be obtained from an on-the-fly diabaticization. Some promising avenues towards this goal include recent work that proposes circumventing diabaticization altogether (102, 103), and advances in the rapid calculation of quasi-diabatic states as discussed earlier.

5.4. Borrowing limitations from RPMD

Multistate RPMD are extensions of RPMD to systems where multiple electronic states are coupled to nuclear degrees of freedom. The limitations of RPMD must therefore be taken into account: specific concerns include the spurious dynamical frequencies introduced by the spring terms between neighboring beads (104), inaccuracies in describing nuclear correlation functions with non-linear operators (105), and the inability to capture nuclear quantum coherence effects at times $> \beta\hbar$ (44, 46).

6. Outlook

This review introduces readers to the theoretical foundations of the recently developed multistate RPMD methods for the simulation of nonadiabatic reactions in the condensed phase using only classical trajectories in an extended electron-nuclear phase space. The applications discussed here demonstrate the versatility of these multistate path integral methods, and the availability of open-source software will enable broader use (106). The many exciting avenues for future research include ab-initio multistate path integral studies and the derivation of a rigorous nonadiabatic reaction rate theory.

DISCLOSURE STATEMENT

The authors are not aware of any affiliations, memberships, funding, or financial holdings that might be perceived as affecting the objectivity of this review.

ACKNOWLEDGMENTS

The author would like to acknowledge former and current graduate students and postdoctoral scholars who contributed to the body of work included in this review. In addition, the author would like to thank Elliot Eklund for helpful discussions, Prof. Huo and Dr. Chowdhury for sharing data from CS-RPMD simulations used to generate plots in panel (c), Figure 2.

The author acknowledges funding from National Science Foundation Career Award Number CHE1555205 and the U.S. Department of Energy, Office of Basic Energy Sciences, Division of Chemical Sciences, Geosciences and Biosciences through the Nanoporous Materials Genome Center under award number DE-FG02-17ER16362.

LITERATURE CITED

1. Evans RFL, Fan WJ, Chureemart P, Ostler TA, Ellis MOA, Chantrell RW. 2014. Atomistic spin model simulations of magnetic nanomaterials. *J. Phys.: Condens. Matter* 26(10):103202
2. Hammes-Schiffer S. 2001. Theoretical Perspectives on Proton-Coupled Electron Transfer Reactions. *Acc. Chem. Res.* 34(4):273–281
3. Born M, Oppenheimer R. 1927. Zur Quantentheorie der Molekeln. *Ann. Phys. (Berlin)* 389(20):457–484
4. Makri N, Makarov DE. 1995. Tensor propagator for iterative quantum time evolution of reduced density matrices. II. Numerical methodology. *J. Chem. Phys.* 102(11):4611–4618
5. Beck MH, Jäckle A, Worth GA, Meyer HD. 2000. The multiconfiguration time-dependent Hartree (MCTDH) method: A highly efficient algorithm for propagating wavepackets. *Phys. Rep.* 324(1):1–105
6. Wang H, Thoss M. 2003. Multilayer formulation of the multiconfiguration time-dependent Hartree theory. *J. Chem. Phys.* 119(3):1289–1299
7. Bonfanti M, Worth GA, Burghardt I. 2020. Multi-Configuration Time-Dependent Hartree Methods: From Quantum to Semiclassical and Quantum-Classical. *Quantum Chemistry and Dynamics of Excited States* :383–411
8. Greene SM, Batista VS. 2017. Tensor-Train Split-Operator Fourier Transform (TT-SOFT) Method: Multidimensional Nonadiabatic Quantum Dynamics. *J. Chem. Theory Comput.* 13(9):4034–4042
9. Richings G, Polyak I, Spinlove K, Worth G, Burghardt I, Lasorne B. 2015. Quantum dynamics simulations using Gaussian wavepackets: the vMCG method. *Int. Rev. Phys. Chem.* 34(2):269–308
10. Curchod BF, Martinez TJ. 2018. Ab Initio Nonadiabatic Quantum Molecular Dynamics. *Chem. Rev.* 118(7):3305–3336
11. Meyer HD, Miller WH. 1979. A classical analog for electronic degrees of freedom in nonadiabatic collision processes. *J. Chem. Phys.* 70(7):3214–3223
12. Stock G, Thoss M. 1997. Semiclassical description of nonadiabatic quantum dynamics. *Phys. Rev. Lett.* 78(4):578–581
13. Thoss M, Stock G. 1999. Mapping approach to the semiclassical description of nonadiabatic quantum dynamics. *Phys. Rev. A* 59(1):64–79
14. Miller WH. 2001. The semiclassical initial value representation: A potentially practical way

- for adding quantum effects to classical molecular dynamics simulations. *J. Phys. Chem. A* 105(13):2942–2955
15. Sun X, Wang H, Miller WH. 1998. Semiclassical theory of electronically nonadiabatic dynamics: Results of a linearized approximation to the initial value representation. *J. Chem. Phys.* 109(17):7064–7074
 16. Wang H, Sun X, Miller WH. 1998. Semiclassical approximations for the calculation of thermal rate constants for chemical reactions in complex molecular systems. *J. Chem. Phys.* 108(23):9726–9736
 17. Wang H, Song X, Chandler D, Miller WH. 1999. Semiclassical study of electronically nonadiabatic dynamics in the condensed-phase: Spin-boson problem with Debye spectral density. *J. Chem. Phys.* 110(10):4828–4840
 18. Ananth N, Venkataraman C, Miller WH. 2007. Semiclassical description of electronically nonadiabatic dynamics via the initial value representation. *J. Chem. Phys.* 127(8):1–9
 19. Miller WH. 2009. Electronically nonadiabatic dynamics via semiclassical initial value methods. *J. Phys. Chem. A* 113(8):1405–1415
 20. Liu J. 2015. Recent advances in the linearized semiclassical initial value representation/classical Wigner model for the thermal correlation function. *Int. J. Quantum Chem.* 115(11):657
 21. Church MS, Hele TJ, Ezra GS, Ananth N. 2018. Nonadiabatic semiclassical dynamics in the mixed quantum-classical initial value representation. *J. Chem. Phys.* 148(10)
 22. Cotton SJ, Miller WH. 2016. The Symmetrical Quasi-Classical Model for Electronically Non-Adiabatic Processes Applied to Energy Transfer Dynamics in Site-Exciton Models of Light-Harvesting Complexes. *J. Chem. Theory Comput.* 12(3):983–991
 23. Cotton SJ, Miller WH. 2019. Trajectory-adjusted electronic zero point energy in classical Meyer-Miller vibronic dynamics: Symmetrical quasiclassical application to photodissociation. *J. Chem. Phys.* 150(19)
 24. Cotton SJ, Miller WH. 2019. A symmetrical quasi-classical windowing model for the molecular dynamics treatment of non-adiabatic processes involving many electronic states. *J. Chem. Phys.* 150(10):104101
 25. Makri N. 2015. Quantum-classical path integral: A rigorous approach to condensed phase dynamics. *Int. J. Quant. Chem.* 115(18):1209
 26. Kapral R. 2006. Progress in the theory of mixed quantum-classical dynamics. *Ann. Phys. Chem.* 57:129–157
 27. Huo P, Coker DF. 2012. Semi-classical path integral non-adiabatic dynamics: A partial linearized classical mapping Hamiltonian approach. *Mol. Phys.* 110(9-10):1035–1052
 28. Agostini F, Abedi A, Suzuki Y, Min SK, Maitra NT, Gross EKV. 2015. The exact forces on classical nuclei in non-adiabatic charge transfer. *J. Chem. Phys.* 142(8):084303
 29. Tully JC, Pkeston RK. 1971. Trajectory surface hopping approach to nonadiabatic molecular collisions: The reaction of H+ with D2. *J. Chem. Phys.* 55(2):562–572
 30. Tully JC. 1998. Mixed quantum-classical dynamics. *Faraday Discuss.* 110:407–419
 31. Wang L, Akimov A, Prezhdo OV. 2016. Recent Progress in Surface Hopping: 2011–2015. *J. Phys. Chem. Lett.* 7(11):2100–2112
 32. Subotnik JE, Jain A, Landry B, Petit A, Ouyang W, Bellonzi N. 2016. Understanding the Surface Hopping View of Electronic Transitions and Decoherence. *Ann. Phys. Chem.* 67:387–417
 33. Tully JC. 2012. Perspective: Nonadiabatic dynamics theory. *J. Chem. Phys.* 137(22)
 34. Hammes-Schiffer S, Tully JC. 1995. Nonadiabatic transition state theory and multiple potential energy surface molecular dynamics of infrequent events. *J. Chem. Phys.* 103(19):8513–8527
 35. Cao J, Voth GA. 1993. A new perspective on quantum time correlation functions. *J. Chem. Phys.* 99(12):10070–10073
 36. J Cao GV. 1994. The formulation of quantum statistical mechanics based on the Feynman path centroid density. II. Dynamical properties. *J. Chem. Phys.* 100(7):5093

37. Jang S, Voth GA. 1999. A derivation of centroid molecular dynamics and other approximate time evolution methods for path integral centroid variables. *J. Chem. Phys.* 111(6):2371–2384
38. Voth GA. 2007. Path-Integral Centroid Methods in Quantum Statistical Mechanics and Dynamics
39. Craig IR, Manolopoulos DE. 2004. Quantum statistics and classical mechanics: Real time correlation functions from ring polymer molecular dynamics. *J. Chem. Phys.* 121(8):3368–3373
40. Craig IR, Manolopoulos DE. 2005. Chemical reaction rates from ring polymer molecular dynamics. *J. Chem. Phys.* 122(8):084106
41. Habershon S, Manolopoulos DE, Markland TE, Miller III TF. 2013. Ring-polymer molecular dynamics: Quantum effects in chemical dynamics from classical trajectories in an extended phase space. *Ann. Phys. Chem.* 64:387–413
42. Feynman RP, Hibbs AR. 1965. *Quantum Mechanics and Path Integrals*. Mc-Graw Hill College, 1st ed.
43. Chandler D, Wolynes PG. 1981. Exploiting the isomorphism between quantum theory and classical statistical mechanics of polyatomic fluids. *J. Chem. Phys.* 74(7):4078–4095
44. Miller III TF. 2008. Isomorphic classical molecular dynamics model for an excess electron in a supercritical fluid. *J. Chem. Phys.* 129(19)
45. Menzeleev AR, Miller III TF. 2010. Ring polymer molecular dynamics beyond the linear response regime: Excess electron injection and trapping in liquids. *J. Chem. Phys.* 132(3)
46. Menzeleev AR, Ananth N, Miller III TF. 2011. Direct simulation of electron transfer using ring polymer molecular dynamics: Comparison with semiclassical instanton theory and exact quantum methods. *J. Chem. Phys.* 135(7):1–18
47. Boekelheide N, Salomón-Ferrer R, Miller III TF. 2011. Dynamics and dissipation in enzyme catalysis. *Proc. Natl. Acad. Sci. U.S.A.* 108(39):16159–16163
48. Kenion RL, Ananth N. 2016. Direct simulation of electron transfer in the cobalt hexamine(II/III) self-exchange reaction. *Phys. Chem. Chem. Phys.* 18(37):26117–26124
49. Kretchmer JS, Miller III TF. 2017. Kinetically-constrained ring-polymer molecular dynamics for non-adiabatic chemistries involving solvent and donor–acceptor dynamical effects. *Faraday Discuss.* 195(0):191–214
50. Ananth N. 2013. Mapping variable ring polymer molecular dynamics: A path-integral based method for nonadiabatic processes. *J. Chem. Phys.* 139(12)
51. Duke JR, Ananth N. 2015. Simulating Excited State Dynamics in Systems with Multiple Avoided Crossings Using Mapping Variable Ring Polymer Molecular Dynamics. *J. Phys. Chem. Lett.* 6(21):4219–4223
52. Pierre S, Duke JR, Hele TJ, Ananth N. 2017. A mapping variable ring polymer molecular dynamics study of condensed phase proton-coupled electron transfer. *J. Chem. Phys.* 147(23)
53. Ranya S, Ananth N. 2020. Multistate ring polymer instantons and nonadiabatic reaction rates. *J. Chem. Phys.* 152(11)
54. Eklund EC, Ananth N. 2021. Investigating the Stability and Accuracy of a Classical Mapping Variable Hamiltonian for Nonadiabatic Quantum Dynamics. *Regul. Chaotic Dyn.* 26(2):131–146
55. Richardson JO, Thoss M. 2013. Communication: Nonadiabatic ring-polymer molecular dynamics. *J. Chem. Phys.* 139(3):031102
56. Richardson JO, Meyer P, Pleinert MO, Thoss M. 2017. An analysis of nonadiabatic ring-polymer molecular dynamics and its application to vibronic spectra. *Chem. Phys.* 482:124–134
57. Chowdhury SN, Huo P. 2019. State dependent ring polymer molecular dynamics for investigating excited nonadiabatic dynamics. *J. Chem. Phys.* 150(24):244102
58. Chowdhury SN, Huo P. 2021. Non-adiabatic Matsubara dynamics and non-adiabatic ring-polymer molecular dynamics. *J. Chem. Phys.* 154(12):124124
59. Chowdhury SN, Huo P. 2017. Coherent state mapping ring polymer molecular dynamics for

- non-adiabatic quantum propagations. *J. Chem. Phys.* 147(21)
60. Domcke W, Yarkony DR. 2012. Role of conical intersections in molecular spectroscopy and photoinduced chemical dynamics. *Ann. Phys. Chem.* 63:325–352
 61. Nakamura H, Truhlar DG. 2001. The direct calculation of diabatic states based on configurational uniformity. *J. Chem. Phys.* 115(22):10353
 62. Baer M. 2002. Introduction to the theory of electronic non-adiabatic coupling terms in molecular systems. *Phys. Rep.* 358(2):75–142
 63. Nakamura H, Truhlar DG. 2002. Direct diabaticization of electronic states by the fourfold way. II. Dynamical correlation and rearrangement processes. *J. Chem. Phys.* 117(12):5576
 64. Wu Q, Van Voorhis T. 2006. Constrained density functional theory and its application in long-range electron transfer. *J. Chem. Theory Comput.* 2(3):765–774
 65. Sirjoosingh A, Hammes-Schiffer S. 2011. Diabatization schemes for generating charge-localized electron-proton vibronic states in proton-coupled electron transfer systems. *J. Chem. Theory Comput.* 7(9):2831–2841
 66. Subotnik JE, Alguire EC, Ou Q, Landry BR, Fatehi S. 2015. The Requisite Electronic Structure Theory To Describe Photoexcited Nonadiabatic Dynamics: Nonadiabatic Derivative Couplings and Diabatic Electronic Couplings. *Acc. Chem. Res.* 48(5):1340–1350
 67. Yarkony DR, Xie C, Zhu X, Wang Y, Malbon CL, Guo H. 2019. Diabatic and adiabatic representations: Electronic structure caveats. *Comput. Theor. Chem.* 1152:41–52
 68. Mao Y, Montoya-Castillo A, Markland TE. 2020. Excited state diabaticization on the cheap using DFT: Photoinduced electron and hole transfer. *J. Chem. Phys.* 153(24):244111
 69. Richings GW, Habershon S. 2020. A new diabaticization scheme for direct quantum dynamics: Procrustes diabaticization. *J. Chem. Phys.* 152(15):154108
 70. Liu J. 2016. A unified theoretical framework for mapping models for the multi-state Hamiltonian. *J. Chem. Phys.* 145(20)
 71. Runeson JE, Richardson JO. 2019. Spin-mapping approach for nonadiabatic molecular dynamics. *J. Chem. Phys.* 151(4)
 72. Polley K, Loring RF. 2020. Spectroscopic response theory with classical mapping Hamiltonians. *J. Chem. Phys.* 153(20):204103
 73. Huo P, Miller III TF, Coker DF. 2013. Communication: Predictive partial linearized path integral simulation of condensed phase electron transfer dynamics. *J. Chem. Phys.* 139(15)
 74. Meyer HD, Miller WH. 1979. Classical models for electronic degrees of freedom: Derivation via spin analogy and application to $F^*+H_2 \rightarrow F+H_2$. *J. Chem. Phys.* 71(5):2156–2169
 75. Trotter HF. 1959. On the product of semi-groups of operators. *Proc. Amer. Math. Soc.* 10(4):545–545
 76. Suzuki M. 1976. Generalized Trotter’s formula and systematic approximants of exponential operators and inner derivations with applications to many-body problems. <https://doi.org/10.1080/00137907608938637>
 77. Chandler D. 1978. Statistical mechanics of isomerization dynamics in liquids and the transition state approximation. *J. Chem. Phys.* 68(6):2959–2970
 78. Parrinello M, Rahman A. 1984. Study of an F center in molten KCl. *J. Chem. Phys.* 80(2):860
 79. Ananth N, Miller III TF. 2010. Exact quantum statistics for electronically nonadiabatic systems using continuous path variables. *J. Chem. Phys.* 133(23)
 80. Chandler D. 1987. *Introduction to Modern Statistical Mechanics*. Oxford University Press (OUP)
 81. DM Ceperley GJ. 1987. Calculation of exchange frequencies in bcc He3 with the path-integral Monte Carlo method. *Phys. Rev. Lett.* 58(16):1648
 82. Kubo R. 1957. Statistical Mechanical Theory of Irreversible Processes. I. General Theory and Simple Applications to Magnetic and Conduction Problems. *J. Phys. Soc. Jpn.* 12(6):570–586
 83. Zwanzig R. 1965. Time-Correlation Functions and Transport Coefficients in Statistical Mechanics. *Ann. Phys. Chem.* 16(1):67–102

84. Golosov AA, Reichman DR. 2001. Classical mapping approaches for nonadiabatic dynamics: Short time analysis. *J. Chem. Phys.* 114(3):1065
85. Habershon S, Manolopoulos DE, S Habershon DM. 2009. Zero point energy leakage in condensed phase dynamics: An assessment of quantum simulation methods for liquid water. *J. Chem. Phys.* 131(24):244518
86. Hele TJ, Althorpe SC. 2013. Derivation of a true ($t \rightarrow 0+$) quantum transition-state theory. I. Uniqueness and equivalence to ring-polymer molecular dynamics transition-state-theory. *J. Chem. Phys.* 138(8):084108
87. Hele TJ, Althorpe SC. 2013. Derivation of a true ($t \rightarrow 0+$) quantum transition-state theory. II. Recovery of the exact quantum rate in the absence of recrossing. *J. Chem. Phys.* 139(8):084115
88. Althorpe SC. 2021. Path-integral approximations to quantum dynamics — SpringerLink. *Eur. Phys. J. B* 94(7):1–17
89. Mean Field RPMD. ???? This method has been used previously by multiple researchers to benchmark nonadiabatic path integral methods including D. E. Manolopoulos, J. C. Tully, I. R. Craig, T. J. H. Hele, N. Ananth, and T. F. Miller III.
90. Hele TJ, Willatt MJ, Muolo A, Althorpe SC. 2015. Communication: Relation of centroid molecular dynamics and ring-polymer molecular dynamics to exact quantum dynamics. *J. Chem. Phys.* 142(19):191101
91. Hele TJ, Ananth N. 2016. Deriving the exact nonadiabatic quantum propagator in the mapping variable representation. *Faraday Discuss.* 195:269–289
92. Hele TJ, Willatt MJ, Muolo A, Althorpe SC. 2015. Boltzmann-conserving classical dynamics in quantum time-correlation functions: "Matsubara dynamics". *J. Chem. Phys.* 142(13):134103
93. Welsch R, Song K, Shi Q, Althorpe SC, Miller III TF. 2016. Non-equilibrium dynamics from RPMD and CMD. *J. Chem. Phys.* 145(20):204118
94. Bonella S, Coker DF. 2003. Semiclassical implementation of the mapping Hamiltonian approach for nonadiabatic dynamics using focused initial distribution sampling. *J. Chem. Phys.* 118(10):4370–4385
95. Colbert DT, Miller WH. 1998. A novel discrete variable representation for quantum mechanical reactive scattering via the S-matrix Kohn method. *J. Chem. Phys.* 96(3):1982–1991
96. Steele RP, Zwickl J, Shushkov P, Tully JC. 2011. Mixed time slicing in path integral simulations. *J. Chem. Phys.* 134(7):074112
97. Coronado EA, Xing J, Miller WH. 2001. Ultrafast non-adiabatic dynamics of systems with multiple surface crossings: a test of the Meyer–Miller Hamiltonian with semiclassical initial value representation methods. *Chem. Phys. Lett.* 349(5-6):521–529
98. Tao X, Shushkov P, Miller III TF. 2019. Simple Flux-Side Formulation of State-Resolved Thermal Reaction Rates for Ring-Polymer Surface Hopping. *J. Phys. Chem. A* 123(13):3013–3020
99. Menzeleev AR, Bell F, Miller III TF. 2014. Kinetically constrained ring-polymer molecular dynamics for non-adiabatic chemical reactions. *J. Chem. Phys.* 140(6)
100. Kretchmer JS, Miller III TF. 2016. Tipping the Balance between Concerted versus Sequential Proton-Coupled Electron Transfer. *Inorg. Chem.* 55(3):1022–1031
101. Duke JR, Ananth N. 2016. Mean field ring polymer molecular dynamics for electronically nonadiabatic reaction rates. *Faraday Discuss.* 195(Cmd):253–268
102. Mandal A, Yamijala SS, Huo P. 2018. Quasi-Diabatic Representation for Nonadiabatic Dynamics Propagation. *J. Chem. Theory Comput.* 14(4):1828–1840
103. Zhou W, Mandal A, Huo P. 2019. Quasi-Diabatic Scheme for Nonadiabatic On-the-Fly Simulations. *J. Phys. Chem. Lett.* 10(22):7062–7070
104. Habershon S, Fanourgakis GS, Manolopoulos DE. 2008. Comparison of path integral molecular dynamics methods for the infrared absorption spectrum of liquid water. *J. Chem. Phys.* 129(7):074501
105. Horikoshi A, Kinugawa K. 2005. Effective potential analytic continuation approach for real

- time quantum correlation functions involving nonlinear operators. *J. Chem. Phys.* 122(17)
106. Eklund EC, Ananth N. 2020. MAVARIC: a C++ program used to compute Mapping Variable Ring Polymer Molecular Dynamics correlation functions. <https://doi.org/10.5281/zenodo.3900570>